(Preprint) AAS 22-152

RELATIVE NAVIGATION AND POINTING ERROR BUDGET FOR AN X-RAY ASTRONOMY FORMATION-FLYING MISSION

Shane Lowe,[*] Maxim Markevitch,[†] and Simone D'Amico[‡]

This paper presents an error budget for the relative navigation and intersatellite pointing of a novel formation-flying mission, Cal X-1. Despite extensive ground calibration campaigns, cross-comparison of orbiting X-ray observatories reveals systematic discrepancies in measured celestial source fluxes of more than 10%. The Cal X-1 mission will address this problem by establishing an in-orbit X-ray flux standard using a pair of SmallSats flying in formation. The first spacecraft will host an X-ray telescope while the second spacecraft will host an absolutely calibrated X-ray source. The mission design requires precise inter-satellite pointing, but constraints on size, weight, power, and cost preclude the use of specialized hardware. This paper seeks to demonstrate that meeting the challenging inter-satellite pointing requirements is feasible through advanced relative navigation techniques. The performance of a suitable relative navigation system is demonstrated in high fidelity simulation. Next, a mathematical model which accounts for errors stemming from relative navigation, attitude determination, and the spacecraft structural assembly is developed to allow the computation of a pointing knowledge error. By comparing this pointing knowledge error with the requirements of the Cal X-1 mission, the feasibility of the proposed inter-satellite pointing methodology is demonstrated.

INTRODUCTION

Concurrently with the steady growth of interest in spacecraft formation-flying and the advent of new commercial satellite constellations, investigations into the enabling technology of inter-satellite pointing have gained increasing relevance. Inter-satellite pointing here refers broadly to the acquisition and maintenance of the mutual alignment of two or more spacecraft. Past and potential future applications of inter-satellite pointing include (1) a variety of science missions, including Earth observation and astronomy, (2) high-bandwidth free-space optical communication, and (3) inspection using optical cameras for in-orbit servicing. In contrast with the considerable flight heritage of the more general topic of spacecraft formation-flying, comparatively few missions have employed inter-satellite pointing.

Notable among the handful of missions which have demonstrated inter-satellite pointing was the Gravity Recovery and Climate Experiment (GRACE) mission, which launched in 2002. The

[*] Doctoral Candidate, Department of Aeronautics & Astronautics, Stanford University, 496 Lomita Mall, Stanford, California, USA.
[†] Astrophysicist, X-ray Astrophysics Laboratory, NASA Goddard Space Flight Center, 8800 Greenbelt Road, Greenbelt, Maryland, USA.
[‡] Associate Professor, Department of Aeronautics & Astronautics, Stanford University, 496 Lomita Mall, Stanford, California, USA.

twin GRACE spacecraft maintained the precise alignment of their K-band microwave ranging instruments in order to perform their gravimetry mission.[1] Free-space optical communication between spacecraft using lasers has been demonstrated in orbit a number of times, including by the SPOT4 and ARTEMIS spacecraft, which launched in 1998 and 2001, respectively. These spacecraft utilized laser communication to send Earth observation data from SPOT4, in LEO, to ARTEMIS, in GEO.[2] Laser communication terminals developed by Tesat-Spacecom were launched onboard the NFIRE and TerraSAR-X spacecraft in 2007 and demonstrated inter-satellite laser communication in the case where both spacecraft are in LEO.[3]

The literature surrounding inter-satellite pointing is dominated by the application of laser communication. A variety of methods have been proposed to achieve the highly precise pointing, acquisition, and tracking required for laser communication. These methods often rely on the spacecraft exchanging navigation information obtained through global navigation satellite systems (GNSS) to realize a coarse initial alignment. Fine pointing is then achieved through specialized hardware, like gimbals and steering mirrors, and appropriate control methodologies.[4] Recognizing the trend towards the miniaturization of spacecraft, efforts have been made to reduce the considerable size, weight, power, and cost (SWaP-C) requirements of laser communication systems.[5] Although these systems advertise inter-satellite pointing at the level of arcseconds, only the beam itself is pointed with that degree of precision, since their purpose is strictly to serve as a high-bandwidth inter-satellite link. A novel attitude control methodology to enable sub-arcsecond pointing accuracy for a formation-flying mission has been proposed, but with a celestial object as the pointing target rather than the partner spacecraft.[6] Situations in which there is a requirement for precise inter-satellite pointing between other spacecraft components, such as scientific instruments, are not addressed in the literature. This is the case for the Cal X-1 mission, which will serve as the reference for the analysis in this paper.

This paper will seek to demonstrate the feasibility of achieving precise inter-satellite pointing without a requirement for specialized hardware by instead relying on relative navigation using differential GNSS (dGNSS) techniques. By doing this, two limitations in the current state of the art will be addressed. First, by eschewing any specialized hardware, the proposed method could be utilized by missions with significant SWaP-C constraints. Second, the proposed method permits the precise mutual alignment of arbitrary locations on or within a pair of spacecraft, so long as those locations are known with respect to other spacecraft components. In order to maintain the focus on precise relative navigation as an enabling technology for inter-satellite pointing, attitude control will not be addressed in this paper. Instead, feasibility will be established by demonstrating an obtainable pointing knowledge error that is well below the pointing accuracy requirement.

Following this introduction, the Cal X-1 mission will be presented and its pointing requirements discussed. Next, the performance of a state-of-the-art relative navigation system, the Distributed Multi-GNSS Timing and Localization (DiGiTaL) system, will be demonstrated in an orbit scenario which is representative of the Cal X-1 mission to inform the later development of the pointing error budget. The subsequent section will present a mathematical model to be used in the computation of the pointing error contribution of relative navigation and other pointing error sources. Next, the pointing error budget will be presented. Finally, the conclusion will summarize the results of this paper and discuss potential future work.

CAL X-1 MISSION

Large orbiting X-ray telescopes are now making observations capable of answering fundamental physics and cosmology questions, such as constraining the density and the expansion rate of the Universe, determining the equation of state of the ultra-dense matter of neutron stars, and studying

the physics of black holes. However, those studies are limited by the lack of absolute X-ray flux calibration; the most powerful X-ray observatories reveal discrepancies in the absolute source fluxes at the 10-20% level. These discrepancies are plausibly related to changes in the instrument performance between the ground calibration and the orbit.

A formation-flying mission, Cal X-1, is proposed to overcome this problem by establishing "standard candles" in the X-ray sky. Cal X-1 will consist of two SmallSats flying in formation. The first, Cal-T, will have a small X-ray telescope and the second, Cal-S, a pair of absolutely calibrated X-ray sources (E=1.5 keV and 6 keV) with internal flux standards. The satellites will be separated in orbit by 2-4 km in order for the optical effect of the finite distance between the sources and the telescope to be negligible. Cal-T will point its telescope alternately toward the Cal-S sources and toward several well-chosen non-variable X-ray sources in the sky. Because the brightness of the Cal-S sources is accurately known, the celestial source fluxes could be calibrated in this manner to a 1-2% uncertainty at each of the two energies, yielding a ten-fold improvement from the current accuracy. Those sources will then become standard X-ray candles for all other X-ray observatories, current and future, to use for calibration of their telescopes in orbit. If Cal X-1 succeeds, it will greatly increase the scientific output of current and planned flagship X-ray observatories like Chandra, XMM-Newton, and eROSITA.

The idea of this measurement imposes strict requirements on the Cal X-1 instruments and spacecraft. The distance between Cal-T and Cal-S can vary but must be known at any moment to within 1 m (1-sigma) to convert the Cal-S source brightness to the incident flux at the telescope aperture. The Cal-T X-ray mirror has a special design to minimize the dependence of the observed source flux on deviations of the source from the telescope axis. To further reduce the observed flux variations, Cal-T must be pointed directly at the source to better than 10 arcseconds (1-sigma) accuracy. When Cal-T is observing the celestial source, which is fixed in the inertial frame, the spacecraft star trackers and attitude determination and control system (ADCS) are capable of this accuracy. However, Cal-S is moving in the sky at an angular speed of 4 arcminutes per second (with the two satellites operating in the low-Earth orbit). Cal-T must be able to track this moving target with the same 10 arcsecond accuracy.

The Cal-T ADCS is capable of following the target at such rate, provided it knows where to point in the inertial frame. A method is needed to determine the instantaneous vector from Cal-T to Cal-S and translate that into commands for the ADCS. The pointing accuracy requirement of 10 arcseconds at the spacecraft separation of 1 km, the lower bound for Cal X-1 operations, corresponds to a 5 cm transverse displacement between the satellites. This is beyond the nominal capabilities of the onboard GNSS receivers, but within the capabilities of advanced dGNSS techniques, which will be employed by the Cal X-1 mission.

RELATIVE NAVIGATION PERFORMANCE

This section will provide a brief overview of the capabilities and key design elements of the Distributed Multi-GNSS Timing and Localization (DiGiTaL) relative navigation system, which will be employed by the Cal X-1 mission. Next, the performance of DiGiTaL in an absolute and relative orbit scenario representative of the Cal X-1 mission will be demonstrated in high fidelity simulation. This demonstrated performance will be used in a subsequent section to inform the development of a pointing error budget and the mission design.

Distributed Multi-GNSS Timing and Localization

The DiGiTaL system was developed by the Stanford Space Rendezvous Laboratory (SLAB) to enable precise relative navigation of arbitrarily sized spacecraft swarms. DiGiTaL achieves this using an unscented Kalman filter (UKF) and dGNSS techniques, which leverage combinations of

raw pseudorange and carrier phase measurements exchanged between spacecraft to cancel common errors.[7,8] DiGiTaL performs integer ambiguity resolution (IAR) onboard in real time to permit full use of low noise carrier phase measurements and achieve relative navigation accuracy at the centimeter level. IAR has been demonstrated extensively for post-facto relative navigation, notably by the GRACE mission.[9] However, by providing this capability in real time, DiGiTaL represents the state of the art in precision GNSS-based relative navigation.

Crucially, the use of DiGiTaL does not require the accommodation of any specialized hardware and is sufficiently computationally efficient to be used by SmallSats with limited onboard processing capabilities.[7] Each spacecraft is only required to host a GNSS receiver and an inter-satellite link must be available to exchange pseudorange and carrier phase measurements, along with auxiliary data.

Simulation Setup

Also developed by SLAB, the Space Rendezvous Lab Satellite Software (***S***^{3}) is a custom software library for high fidelity dynamic simulation. ***S***^{3} has been validated extensively through comparison with flight data from the PRISMA mission and is used in this analysis to provide the ground-truth orbit simulation data.[10]

Table 1. Simulation Force Models, Corrections, and Reference Frames.

Perturbation/Transformation	Model
Equations of motion	Fundamental orbital differential equation
Numerical integrator	Fourth-order Runge-Kutta[11] Richardson extrapolation[12]
Gravity field	GRACE Gravity Model GGM01S[13]
Atmospheric drag	NRLMSISE-00[14]
Solar radiation pressure	Conical Earth shadow model[10]
Geomagnetic and solar flux data	NOAA daily KP AP indices
Third-body gravity	Analytical Sun and Moon[10]

The models used by ***S***^{3} to generate the ground-truth orbit data for this simulation are shown in Table 1. The Earth-centered inertial (ECI) reference frame used in this simulation and subsequent analysis is defined as J2000 and the Earth-centered Earth-fixed (ECEF) reference frame used is WGS84. Additionally, ***S***^{3} uses a NovAtel OEM628 GNSS Receiver Emulator, which provides pseudorange and carrier phase measurements with Gaussian white noise of 20 cm and 1 mm, respectively.[15] The GNSS ephemerides from archived International GNSS Service data are used for measurement generation, while broadcast ephemerides with meter-level error are provided to the DiGiTaL software.

Table 2. Simulation Spacecraft Parameters.

	Cal-S	Cal-T
Mass (kg)	24	12
$\boldsymbol{A_{drag}}$ $(\mathbf{m^2})$	0.06	0.64
$\boldsymbol{A_{srp}}$ $(\mathbf{m^2})$	0.06	0.64
$\boldsymbol{C_d}$	2.0	2.0
$\boldsymbol{C_r}$	1.8	1.8

The physical parameters for the Cal-S and Cal-T spacecraft used in simulation are shown in Table 2.

Table 3. Simulation Absolute Orbit.

a (km)	e	i	Ω	ω
6853.137	0.001	28°	0	0

Cal-S is designated to be the Chief spacecraft for this simulation. The parameterization of its absolute orbit in terms of classical Keplerian orbital elements is shown in Table 3. The absolute orbit represents a near-circular, inclined orbit at an altitude of 475 km. This orbit was chosen based on the formation requirements and the desired mission lifetime.[16]

Table 4. Simulation Relative Orbit.

$a\delta a$	$a\delta\lambda$	$a\delta e_x$	$a\delta e_y$	$a\delta i_x$	$a\delta i_y$
0	4000 m	0	0	0	0

The parameterization of the relative orbit of Cal-T with respect to Cal-S in relative orbital elements is shown in Table 4. Relative orbital elements are a non-linear combination of the classical Keplerian orbital elements.[17] They are slowly varying compared to Cartesian representations of the relative state, thereby easing numerical integration for state propagation, and they provide straightforward geometric insight into the spacecraft relative motion. The relative orbit chosen for this simulation represents a purely along-track separation between Cal-S and Cal-T of 4 km.

Simulation Results

The orbits of both spacecraft are simulated for 4 hours, comprising approximately 2.5 orbits. This simulation duration ensures that the DiGiTaL navigation filter is able to reach a steady state and successfully perform IAR, thereby providing the most accurate representation of its nominal performance.

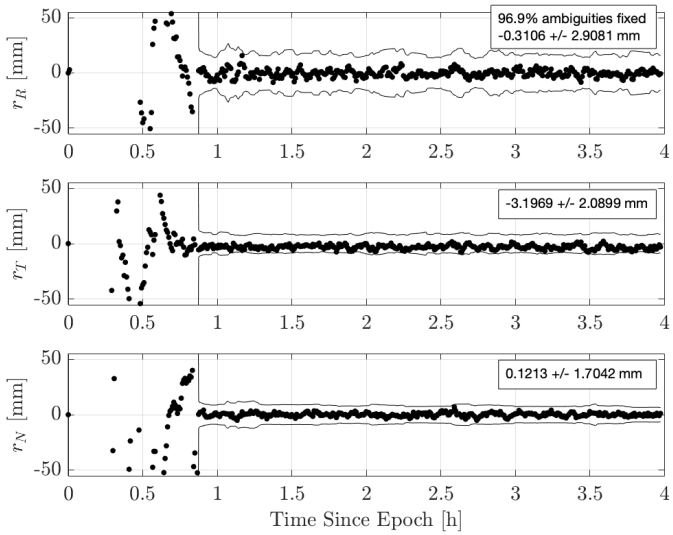

Figure 1. Relative Position Estimation Error in the RTN frame.

Figure 1 shows the relative position estimation error in each component of the local radial-tangential-normal (RTN) frame. Note that, after approximately 45 minutes of simulation time, the relative navigation accuracy improves dramatically. This behavior is due to the successful resolution of integer ambiguities and is consistent with previously published results for the performance of DiGiTaL.[10] Over the last orbit of the simulation the 3D root mean square (RMS) error for the relative position estimation is 5.0964 mm. This 3D RMS error figure will be used in the subsequent development of the pointing error budget with proper offsets for margin and contingency.

POINTING ERROR MODELING

In this section the key reference frames and vectors that will be used in the analysis are defined and a simple mathematical model is developed in order compute the pointing knowledge error due to various sources, including the structural assembly, attitude estimation, and relative navigation.

Reference Frames

There are four reference frames used in this analysis. The first two reference frames are body-fixed frames corresponding to the Cal-S and Cal-T spacecraft. These are shown in Figure 2 as a set of orange and a set of green axes with directions $\hat{x}$, $\hat{y}$, and $\hat{z}$. Each of these sets of axes forms a right-handed triad. The use of reference frames that are fixed to the spacecraft bodies is motivated by the need to know the position and orientation of various spacecraft components with respect to one another. The body-fixed frame provides a convenient means of describing these relationships. The subscripts s and t are applied to the axis labels of the body-fixed frames to indicate their applicability to Cal-S and Cal-T, respectively.

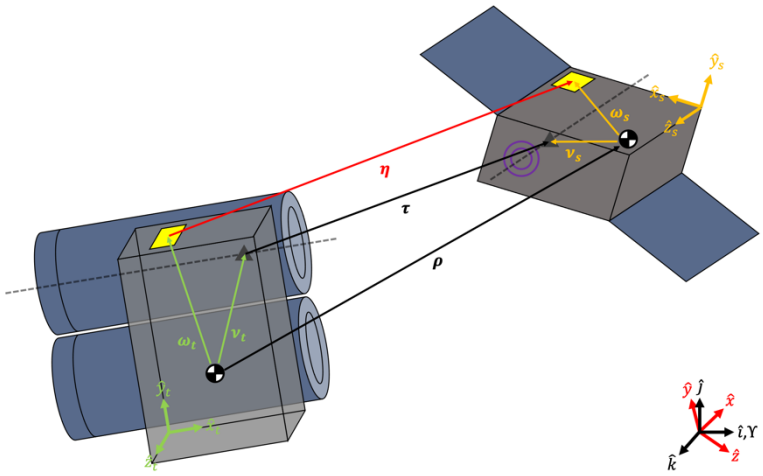

Figure 2. Sketch of Cal X-1 Pointing Scenario.

The third reference frame is the Earth-centered Earth-fixed (ECEF) frame, which is shown as a set of red axes with directions $\hat{x}$, $\hat{y}$, and $\hat{z}$. The ECEF frame is the reference frame used by the Global Positioning System (GPS), and its use in this model is motivated by the dependency of Cal X-1's navigation on GNSS-based navigation. As before, the specific realization of the ECEF frame that will be used is WGS84. The final reference frame is the Earth-centered inertial (ECI) reference frame, which is shown as a set of black axes with directions $\hat{\imath}$, $\hat{\jmath}$, and $\hat{k}$. Similarly to the ECEF frame, the ECI frame is centered at Earth's center of mass. The use of the ECI frame is motivated by the functionality provided by spacecraft star trackers, which is to determine attitude with respect to celestial objects, as well as the dependency of the dynamics model and equations of motion on the inertial frame. The specific realization of the ECI used is J2000. All rotations between reference frames are defined in $\mathbb{R}^3 \; x \; \mathbb{R}^3$.

Vectors

Several important vectors are also shown in Figure 2. The vector $\boldsymbol{\eta}$ points from the phase center of the GNSS antenna onboard Cal-T to the phase center of the GNSS antenna onboard Cal-S. GNSS measurements refer to the ECEF frame. However, the dynamics models which are used for navigation refer to the ECI frame. It is important to note that GNSS measurements obtained onboard in the ECEF frame will be modeled in the ECI frame for navigation purposes, necessitating a transformation between the two frames. The vector $\boldsymbol{\rho}$ points from the center of mass of Cal-T to the center of mass of Cal-S. This vector is estimated as an output of the onboard relative navigation system in the ECI frame. The vector $\boldsymbol{\tau}$ points from a location of relevance to the optics of the telescope onboard Cal-T to the corresponding point of the X-ray source onboard Cal-S. For Cal-T, this location is within the telescope, approximately 10 cm away from the exterior surface and along the boresight. For Cal-S, it is at a comparable location but instead only 1 cm from the exterior surface. Obtaining the error in this vector as an angular measurement is the ultimate goal of the pointing error model.

The vectors $\boldsymbol{\omega}_s$ and $\boldsymbol{\omega}_t$ point from the centers of mass of the spacecraft to their respective GNSS antennas in the body-fixed frame. The vectors $\boldsymbol{\nu}_s$ and $\boldsymbol{\nu}_t$ point from the centers of mass of the spacecraft to their respective instruments in the body-fixed frame. For Cal-S this instrument is the X-ray source and for Cal-T it is the telescope. The center of mass of the spacecraft is used as a common origin for these vectors because the orbital and attitude dynamics refer to the center of mass. However, there is uncertainty in knowledge of the location of the center of mass which must

be accounted for. In other words, there is a vector from the true center of mass to the estimated center of mass, just as there is a vector from the true phase center of the GNSS antenna to the estimated phase center and a vector from the true locations of interest for the telescope and X-ray source and the estimated locations. All vectors appearing in this analysis are defined in $\mathbb{R}^3$.

Mathematical Model Development

An equation for $\boldsymbol{\tau}$ is formed using the appropriate vector addition, with reference to Figure 2, as

$$\boldsymbol{\tau}^{ECI} = \boldsymbol{\rho}^{ECI} + \boldsymbol{\nu}_s{}^{ECI} - \boldsymbol{\nu}_t{}^{ECI} \tag{1}$$

However, $\boldsymbol{\nu}_s$ and $\boldsymbol{\nu}_t$ are known in the body-fixed (BF) frame and must be rotated into the ECI frame

$$\boldsymbol{\tau}^{ECI} = \boldsymbol{\rho}^{ECI} + {}^{BF}\boldsymbol{R}_s^{ECI}\boldsymbol{\nu}_s{}^{BF} - {}^{BF}\boldsymbol{R}_t^{ECI}\boldsymbol{\nu}_t{}^{BF} \tag{2}$$

Here ${}^{BF}\boldsymbol{R}_i^{ECI}$ is the rotation matrix from the body-fixed frame to the ECI frame for spacecraft *i*. This rotation represents the spacecraft's attitude estimation. The development of $\boldsymbol{\rho}$ follows the same methodology as in Eq. 1

$$\boldsymbol{\rho}^{ECI} = \boldsymbol{\eta}^{ECI} + \boldsymbol{\omega}_t{}^{ECI} - \boldsymbol{\omega}_s{}^{ECI} \tag{3}$$

As before, the vectors are not known in the desired frame. In this case, $\boldsymbol{\eta}$ is known in the ECEF frame and $\boldsymbol{\omega}_s$ and $\boldsymbol{\omega}_t$ are known in the body-fixed frame

$$\boldsymbol{\rho}^{ECI} = {}^{ECEF}\boldsymbol{R}^{ECI}\boldsymbol{\eta}^{ECEF} + {}^{BF}\boldsymbol{R}_s^{ECI}\boldsymbol{\omega}_s^{BF} - {}^{ECEF}\boldsymbol{R}_t^{ECI}\boldsymbol{\omega}_t^{BF} \tag{4}$$

Our goal is not the computation of these vectors, however, but their error. It is necessary, then, to define a function $\epsilon(\cdot)$ to represent these errors. The domain of $\epsilon(\cdot)$ consists of vectors representing Cartesian relative positions and rotation matrices. In the case of the former, the codomain is a scalar quantity computed as the L_2 norm of the difference between the true vector and the estimated vector. For example, the error in $\boldsymbol{\eta}$ will be computed as

$$\epsilon(\boldsymbol{\eta}) = \|\boldsymbol{\eta}_{true} - \boldsymbol{\eta}_{est}\|_2 \tag{5}$$

For rotation matrices, the codomain of $\epsilon(\cdot)$ is also a scalar quantity representing the largest single-axis angular difference between the true rotation matrix and the estimated rotation matrix. For example, if the rotation matrix $\boldsymbol{R}_{est}$ differs from the true rotation matrix $\boldsymbol{R}_{true}$ by a set of rotations about each axis of its coordinate system, given by Euler angles ψ, θ, and φ, then the error in the rotation matrix will be

$$\epsilon(\boldsymbol{R}) = max\{\psi, \theta, \varphi\} \tag{6}$$

Thus, the output of $\epsilon(\cdot)$ is always a scalar quantity. Returning to the development of the model, the error in $\boldsymbol{\tau}$ can be expressed as a function of the errors of the constituent terms in Eq. (2)

$$\epsilon(\boldsymbol{\tau}^{ECI}) = f\left(\epsilon(\boldsymbol{\rho}^{ECI}), \epsilon({}^{BF}\boldsymbol{R}_s^{ECI}\boldsymbol{\nu}_s^{BF}), \epsilon({}^{BF}\boldsymbol{R}_t^{ECI}\boldsymbol{\nu}_t^{BF})\right) \tag{7}$$

The error in $\boldsymbol{\rho}$ can then be similarly expressed as a function of the errors in the constituent terms of Eq. (4)

$$\epsilon(\boldsymbol{\rho}^{ECI}) = g\left(\epsilon({}^{ECEF}\boldsymbol{R}^{ECI}\boldsymbol{\eta}^{ECEF}), \epsilon({}^{BF}\boldsymbol{R}_s^{ECI}\boldsymbol{\omega}_s^{BF}), \epsilon({}^{BF}\boldsymbol{R}_t^{ECI}\boldsymbol{\omega}_t^{BF})\right) \tag{8}$$

The second and third terms in Eq. (7) can be further expanded using partial derivatives as

$$\epsilon\left({}^{BF}\boldsymbol{R}_i^{ECI}\boldsymbol{\nu}_i^{BF}\right) = \epsilon\left({}^{BF}\boldsymbol{R}_i^{ECI}\right)\boldsymbol{\nu}_i^{BF} + {}^{BF}\boldsymbol{R}_i^{ECI}\epsilon\left(\boldsymbol{\nu}_i^{BF}\right) \tag{9}$$

Following the same methodology, the individual terms in Eq. (8) can be expanded, which yields the following equations

$$\epsilon({}^{ECEF}\boldsymbol{R}^{ECI}\boldsymbol{\eta}^{ECEF}) = \epsilon\left({}^{BF}\boldsymbol{R}_i^{ECI}\right)\boldsymbol{\omega}_i^{BF} + {}^{BF}\boldsymbol{R}_i^{ECI}\epsilon\left(\boldsymbol{\omega}_i^{BF}\right) \tag{10}$$

$$\epsilon\left({}^{BF}\boldsymbol{R}_i^{ECI}\boldsymbol{\omega}_i^{BF}\right) = \epsilon\left({}^{BF}\boldsymbol{R}_i^{ECI}\right)\boldsymbol{\omega}_i^{BF} + {}^{BF}\boldsymbol{R}_i^{ECI}\epsilon\left(\boldsymbol{\omega}_i^{BF}\right) \tag{11}$$

This expansion by partial derivatives makes the implicit assumptions that errors are random and uncorrelated and thereby ignores any systematic errors. However, this method introduces an inconsistency with the earlier definition of $\epsilon(\cdot)$ by including the products of scalar quantities with vectors and rotation matrices. This will be addressed by treating the vector components of such products as their magnitudes and the rotation matrices as 1-valued scalars. For example, Eq. (11) would become

$$\epsilon\left({}^{BF}\boldsymbol{R}_i^{ECI}\boldsymbol{\omega}_i^{BF}\right) = \epsilon\left({}^{BF}\boldsymbol{R}_i^{ECI}\right)\left\|\boldsymbol{\omega}_i^{BF}\right\|_2 + 1\epsilon\left(\boldsymbol{\omega}_i^{BF}\right) \tag{12}$$

This permits the computation of a scalar quantity that is able to account for the pointing error contribution of the constituent error sources while remaining consistent with the overall pointing error model.

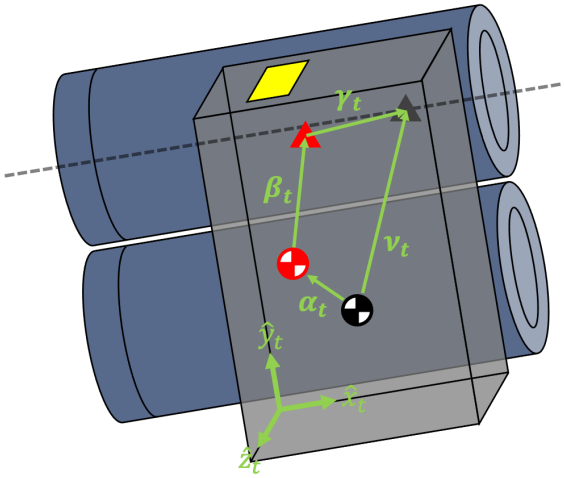

Figure 3. Sketch of Vector from Center of Mass to Optical Center.

Next, several additional vectors are introduced to account for all of the sources of error affecting $\boldsymbol{\nu}_i$. As show in Figure 3, the positions of both the start point of $\boldsymbol{\nu}_i$, the spacecraft center of mass, and the end point, the optical center of the instrument, are uncertain. The true center of mass is shown in black, while the true optical center of the telescope is shown as a dark gray triangle. The estimated locations of these points of interest are shown in red. The vector $\boldsymbol{\alpha}_i$ points from the true center of mass to the estimated center of mass of spacecraft *i*. The vector $\boldsymbol{\beta}_i$ points from the

estimated center of mass to the estimated optical center of the telescope. Finally, $\boldsymbol{\gamma}_i$ points from the estimated to the true optical center. These vectors are shown as applied to Cal-T, but their meaning is identical for Cal-S, swapping the telescope for the X-ray source. Using vector addition, an expression for $\boldsymbol{\nu}_i$ can be formed as

$$\boldsymbol{\nu}_i^{BF} = \boldsymbol{\alpha}_i^{BF} + \boldsymbol{\beta}_i^{BF} + \boldsymbol{\gamma}_i^{BF} \tag{13}$$

As before, the error in $\boldsymbol{\nu}_i$ is a function of the errors in the constituent terms

$$\epsilon\left(\boldsymbol{\nu}_i^{BF}\right) = p\left(\epsilon\left(\boldsymbol{\alpha}_i^{BF}\right), \epsilon\left(\boldsymbol{\beta}_i^{BF}\right), \epsilon\left(\boldsymbol{\gamma}_i^{BF}\right)\right) \tag{14}$$

Here $\epsilon\left(\boldsymbol{\alpha}_i^{BF}\right)$ represents uncertainty in the location of the center of mass, $\epsilon\left(\boldsymbol{\beta}_i^{BF}\right)$ represents uncertainty in the relative position of the optical center with respect to the center of mass, and $\epsilon\left(\boldsymbol{\gamma}_i^{BF}\right)$ represents uncertainty in the location of the optical center. As with $\boldsymbol{\nu}_i$, the analysis of the error sources affecting $\boldsymbol{\omega}_i$ requires the introduction of additional vectors.

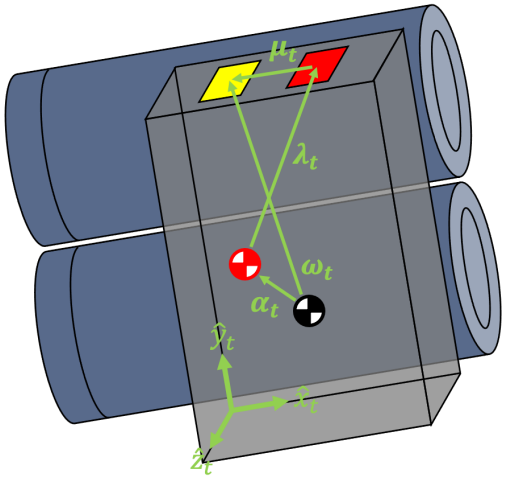

Figure 4. Sketch Vector from Center of Mass to Antenna Phase Center.

In Figure 4 the true location of the GNSS antenna phase center is shown as a yellow parallelogram, while the estimated location is shown as a red parallelogram. The definition of the vector $\boldsymbol{\alpha}_i$ remains the same as before. The vector $\boldsymbol{\lambda}_i$ points from the estimated center of mass to the estimated antenna phase center. The vector $\boldsymbol{\mu}_i$ points from the estimated to the true antenna phase center. As before, these vectors share the same definitions when applied to Cal-S

$$\boldsymbol{\omega}_i^{BF} = \boldsymbol{\alpha}_i^{BF} + \boldsymbol{\lambda}_i^{BF} + \boldsymbol{\mu}_i^{BF} \tag{15}$$

The error affecting $\boldsymbol{\omega}_i$ can then be written as a function of these constituent terms

$$\epsilon\left(\boldsymbol{\omega}_i^{BF}\right) = q\left(\epsilon\left(\boldsymbol{\alpha}_i^{BF}\right), \epsilon\left(\boldsymbol{\lambda}_i^{BF}\right), \epsilon\left(\boldsymbol{\mu}_i^{BF}\right)\right) \tag{16}$$

Next it is necessary to develop the functions $f(\cdot)$, $g(\cdot)$, $p(\cdot)$, and $q(\cdot)$ which will be used to model the level of correlation between individual error sources. It is already assumed that the various error terms are uncorrelated, as previously stated with reference to the expansion of error terms by partial derivatives. Thus, it is appropriate to define all of the functions as addition in quadrature

$$f(\cdot) = g(\cdot) = p(\cdot) = q(\cdot) = \sqrt{\sum \epsilon(\cdot)^2} \tag{17}$$

As the final step, the error in the vector $\boldsymbol{\tau}$ must be converted from a translational error into an angular error. By making the conservative assumption that all of the translational error is perpendicular to the true vector, simple trigonometry permits the computation of the angle subtended by the true vector and the error. Assuming small angles, i.e. $tan(\xi) \approx \xi$, the equivalent pointing knowledge error can then be computed as

$$\xi = \frac{\epsilon(\boldsymbol{\tau}_{est})}{\|\boldsymbol{\tau}_{true}\|_2} \tag{18}$$

POINTING ERROR BUDGET

There are a variety of methodologies in the literature for the development of pointing error budgets, with individual methodologies often being unique to a specific mission.[18] However, certain tools recur frequently in these analyses and efforts have been made to standardize pointing error budget development, notably by the European Space Agency (ESA).[19] This paper has chosen the route taken by many other authors by employing many of the basic tools proposed by the ESA but adapting the process to the specific needs of the Cal X-1 mission. This was done by eschewing the more burdensome mathematical elements, such as the transformations between types of probability distribution functions and the strict definitions of the time-dependency of pointing error sources, which are unnecessary for a feasibility study at this early stage of development.

Table 5. Variable Values.

Variable	Value	Variable	Value
$\|\boldsymbol{\eta}^{ECEF}\|_2$	various	$\epsilon(\boldsymbol{\alpha}_s^{BF})$	0.010 m
$\epsilon(\boldsymbol{\eta}^{ECEF})$	0.005 m	$\epsilon(\boldsymbol{\alpha}_t^{BF})$	0.010 m
$\epsilon({}^{ECEF}\boldsymbol{R}^{ECI})$	1 arcsec	$\epsilon(\boldsymbol{\beta}_s^{BF})$	0.001 m
$\epsilon({}^{BF}\boldsymbol{R}_s^{ECI})$	25 arcsec	$\epsilon(\boldsymbol{\beta}_t^{BF})$	0.001 m
$\epsilon({}^{BF}\boldsymbol{R}_t^{ECI})$	25 arcsec	$\epsilon(\boldsymbol{\gamma}_s^{BF})$	0.001 m
$\|\boldsymbol{\omega}_s^{BF}\|_2$	0.200 m	$\epsilon(\boldsymbol{\gamma}_t^{BF})$	0.001 m
$\|\boldsymbol{\omega}_t^{BF}\|_2$	0.200 m	$\epsilon(\boldsymbol{\lambda}_s^{BF})$	0.001 m
$\|\boldsymbol{\nu}_s^{BF}\|_2$	0.300 m	$\epsilon(\boldsymbol{\lambda}_t^{BF})$	0.001 m
$\|\boldsymbol{\nu}_t^{BF}\|_2$	0.300 m	$\epsilon(\boldsymbol{\mu}_s^{BF})$	0.010 m
		$\epsilon(\boldsymbol{\mu}_t^{BF})$	0.010 m

The values for each term used in the computation of the pointing knowledge error are shown in Table 5. As the Cal X-1 mission is still early in its development, these values are chosen based on the authors' experience regarding the structural assembly of spacecraft and the capabilities of attitude estimation. The exceptions to this are the values for $\epsilon(\boldsymbol{\eta}^{ECEF})$, which was demonstrated in simulation, and $\|\boldsymbol{\eta}^{ECEF}\|_2$, which is varied across the range of expected inter-satellite distances for the Cal X-1 mission.

Table 6. Pointing Error Budget.

$\|\boldsymbol{\eta}^{ECEF}\|_2$ (m)	1000	2000	4000
Pointing Knowledge Error (arcsec)	5.19	2.60	1.30
Pointing Accuracy Requirement (1σ)	10	10	10
Margin	48%	74%	87%

Proceeding with the computation method described in the previous section results in the pointing knowledge error figures shown in Table 6 for various inter-satellite separations. Recall that objective of this analysis was to demonstrate that, through precise relative navigation, a pointing knowledge error could be obtained which is considerably lower than the pointing accuracy requirement of the mission. As expected, at larger inter-satellite distances the impact of translational errors due to structural misalignment on the overall pointing knowledge error are reduced. At 4 km distance the pointing knowledge error is only 1.30 arcseconds, which leaves a margin of 87%. Recognizing that the available margin will be dominated by errors stemming from attitude control, this shows that meeting demanding inter-satellite pointing requirements based on precise relative navigation is achievable.

CONCLUSION

Achieving an inter-satellite pointing accuracy of 10 arcseconds is among the most challenging requirements faced by the Cal X-1 mission. This challenge is compounded by the significant size, weight, power, and cost constraints that preclude the use of specialized hardware onboard the spacecraft. This paper sought to demonstrate the feasibility of meeting this requirement using relative navigation based on global navigation satellite systems (GNSS) performed by the DiGiTaL system. This system employs differential GNSS techniques and integer ambiguity resolution to achieve relative navigation accuracy at the centimeter level while being computationally efficient enough for use onboard SmallSats.

A mathematical model was developed for the pointing knowledge error between the X-ray telescope onboard Cal-T and the X-ray source onboard Cal-S. This model represents a contribution to the literature by providing a method of analysis for pointing between arbitrary locations on spacecraft bodies. Using the model, this paper showed that a pointing knowledge error of 1.30 arcseconds at an inter-satellite distance of 4 km could be achieved, thereby leaving an 87% margin with respect to the pointing accuracy requirement. This promising result demonstrates that achieving precise inter-satellite pointing based on relative navigation is feasible.

Future work should seek to expand upon this analysis in two directions. First, by improving the fidelity of the pointing knowledge error computation by refining the variable values used as the Cal X-1 mission develops further. For example, better information about the structural assembly and its limitations would enhance the overall model fidelity. Second, attitude control should be incorporated into the simulations and error budget development. It is likely that errors resulting from imperfect attitude control will dominate the available margin in the pointing error budget and it is crucial that this contribution to the overall pointing error be quantified. Despite the focus in this paper on the Cal X-1 mission, the method presented is general and is already finding application in the upcoming VIrtual Super Optics Reconfigurable Swarm (VISORS) mission which is due for launch in late 2023 with centimeter-level relative position control requirements at 40 m inter-satellite separation in low Earth orbit.

REFERENCES

[1] Bandikova, T., Flury, J., and Ko, U. "Characteristics and accuracies of the GRACE inter-satellite pointing." *Advances in Space Research*, vol. 50, pp. 123-135, 2021.

[2] Tolker-Nielsen, T. and Oppenhauser, G. "In-orbit test result of an operational optical intersatellite link between ARTEMIS and SPOT4, SILEX." *Free-Space Laser Communication Technologies XIV*, vol. 4635, pp. 1-15. International Society for Optics and Photonics, 2002.

[3] Fields, R., Lunde, C., Wong, R., Wicker, J., Kozlowski, D., Jordan J., Hansen, B., Muehlnikel, G., Scheel, W., Sterr, U., and Kahle, R. "NFIRE-to-TerraSAR-X laser communication results: satellite pointing, disturbances, and other attributes consistent with successful performance." *Sensors and Systems for Space Applications III*, vol. 7330, p. 73300Q. International Society for Optics and Photonics, 2009.

[4] Guelman, M., Kogan, A., Kazarian, A., Livne, A., Orenstein, M., and Michalik, H. "Acquisition and pointing control for inter-satellite laser communications." *IEEE Transactions on Aerospace and Electronic Systems*, vol. 40, pp. 1239-1248, 2004.

[5] Grenfell, P., Aguilar, A., Cahoy, K. and Long, M., 2018. "Pointing, Acquisition, and Tracking for Small Satellite Laser Communications." *32nd Annual AIAA/USU Conference on Small Satellites*, Utah State University, August 7-12 (2018).

[6] Beierle, C., Norton, A., Macintosh, B., and D'Amico, S. "Two-stage attitude control for direct imaging of exoplanets with a CubeSat telescope." *Space Telescopes and Instrumentation 2018: Optical, Infrared, and Millimeter Wave*, vol. 10698, p. 106981Z. International Society for Optics and Photonics, 2018.

[7] Giralo, V. and D'Amico, S. "Distributed multi-GNSS timing and localization for nanosatellites." *NAVIGATION, Journal of the Institute of Navigation*, vol. 66, pp. 729-746, 2019.

[8] Giralo, V. and D'Amico, S. "Precise Real-Time Relative Orbit Determination for Large-Baseline Formations Using GNSS." *Proceedings of the 2021 International Technical Meeting of The Institute of Navigation*, pp. 366-384, 2021.

[9] Laurichesse, D., Mercier, F., Berthias, J.P., Broca, P. and Cerri, L. "Integer ambiguity resolution on undifferenced GPS phase measurements and its application to PPP and satellite precise orbit determination." *Navigation*, vol. 56, no. 2, pp.135-149, 2009.

[10] Giralo, V. "Precision Navigation of Miniaturized Distributed Space Systems Using GNSS." Doctoral Dissertation, Stanford University, 2021.

[11] Montenbruck, O. and Gill, E. *Satellite Orbits*, vol. 2, Springer, 2000.

[12] Montenbruck, O. and Gill, E. "State interpolation for on-board navigation systems." *Aerospace science and technology*, vol. 5, no. 3, pp. 209-220, 2001.

[13] Tapley, B.D., Bettadpur, S., Watkins, M., and Reigber, C. "The gravity recovery and climate experiment: Mission overview and early results." *Geophysical Research Letters*, vol. 31, no. 9, 2004.

[14] Picone, J., Hedin, A., Drop, D.P., and Aikin, A. "NRLMSISE-00 empirical model of the atmosphere: Statistical comparisons and scientific issues." *Journal of Geophysical Research: Space Physics*, vol. 107, no A12, pp. SIA-15, 2002.

[15] Giralo, V. and D'Amico, S. "Development of the Stanford GNSS navigation testbed for distributed space systems." *Proceedings of the 2018 International Technical Meeting of the Institute of Navigation*, pp. 837-856, 2018.

[16] Jahoda, K., Markevitch, M., Okajima, T., Hill-Kittle, J., Shah, N., Bergeron, D., Holland, A., Plucinsky, P. and Schwarz, D. "Cal X-1: an absolute in-orbit calibrator for current and future X-ray observatories."

[17] D'Amico, S. "Autonomous Formation Flying in Low Earth Orbit." Doctoral Dissertation, TU Delft, 2010.

[18] Madni, A., Bradley, N., Cervantes, D., Eldred, D., Oh, D., Mathews, D. and Lai, P.C., "Pointing Error Budget Development and Methodology on the Psyche Project." *2021 IEEE Aerospace Conference,* pp. 1-18, 2021.

[19] Ott, T., Benoit, A., Van den Braembussche, P. and Fichter, W., "ESA Pointing Error Engineering Handbook." *8th International ESA Conference on Guidance, Navigation & Control Systems,* p.17, 2011.